A Nonlocal Unified Variational Framework for Free Surface Flows

SHUSEN LIU, Institute of Software, Chinese Academy of Sciences, China
YUZHONG GUO, Institute of Software, Chinese Academy of Sciences, China
LIXIN REN, Institute of Software, Chinese Academy of Sciences, China
YING QIAO, Institute of Software, Chinese Academy of Sciences, China
XIAOWEI HE*, Institute of Software, Chinese Academy of Sciences, China

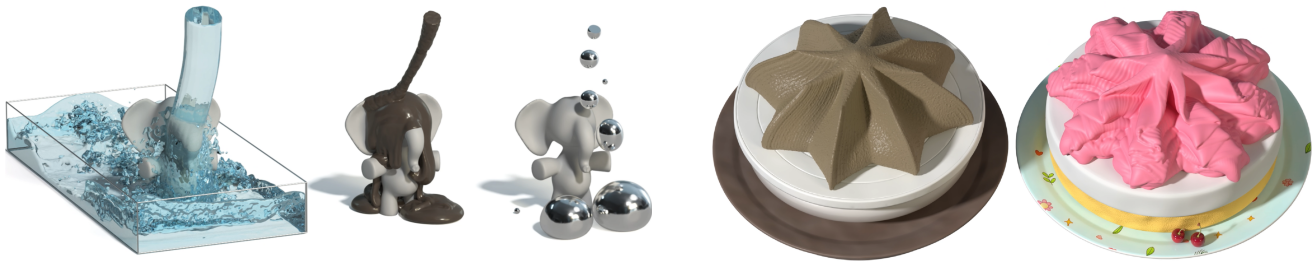

Fig. 1. Our unified method achieves strong coupling among incompressibility, viscosity, and surface tension, significantly enhancing simulation stability for challenging cases such as highly viscous and strongly surface-tension-dominated fluids. (Left) Bathing baby elephant. Diverse fluid behaviors are modeled with our method: low-viscosity flow (661k particles), high-viscosity mud (153k particles), and an extremely high-surface-tension fluid (330k particles). (Right) Mud and cream (1.7M particles per fluid). The mud exhibits high shear viscosity ($\lambda = 1400, \mu = 600$), leading to pronounced expansion under compression; the cream has very low shear viscosity ($\lambda = 2000, \mu = 0$), producing fine and sharp fluid details during squeezing. Owing to the strong coupling between incompressibility and viscosity, both fluids maintain stable shapes.

Simulating free-surface flows requires capturing the effects of incompressibility, viscosity, and surface tension. Existing particle-based methods often rely on operator splitting, which introduces coupling artifacts and limits stability. We propose a unified nonlinear optimization framework that achieves a strong coupling of these three effects within a single solver. By leveraging peridynamics, we formulate the discretization of distinct fluid mechanisms under a consistent variational principle. Specifically, we recast fluid motion as a nonlinear variational optimization problem over particle positions, which is solved via the semi-implicit successive substitution method. Moreover, the framework incorporates separate treatments for bulk and shear viscosity, allowing for more refined control of different viscous fluid behaviors. To the best of our knowledge, this is the first particle-based unified solver capable of fully resolving the interdependence of incompressibility, viscosity, and surface tension, thereby significantly enhancing stability in complex simulations of free-surface flows. The source code for the paper is publicly available at https://github.com/peridyno/peridyno.

CCS Concepts: • **Computing methodologies** → **Physical simulation**.

*Corresponding author.

Authors' Contact Information: Shusen Liu, Institute of Software, Chinese Academy of Sciences, Beijing, China, liushusen@iscas.ac.cn; Yuzhong Guo, Institute of Software, Chinese Academy of Sciences, Beijing, China, guoyuzhong@iscas.ac.cn; Lixin Ren, Institute of Software, Chinese Academy of Sciences, Beijing, China, renlixin@iscas.ac.cn; Ying Qiao, Institute of Software, Chinese Academy of Sciences, Beijing, China, qiaoying@iscas.ac.cn; Xiaowei He, Institute of Software, Chinese Academy of Sciences, Beijing, China, xiaowei@iscas.ac.cn.

SIGGRAPH Conference Papers '26, Los Angeles, CA, USA

ACM ISBN 979-8-4007-2554-8/2026/07
https://doi.org/10.1145/3799902.3811196

Additional Key Words and Phrases: Free surface flow, incompressible fluid, viscous fluid, surface tension, particle-based fluid, peridynamics

ACM Reference Format:
Shusen Liu, Yuzhong Guo, Lixin Ren, Ying Qiao, and Xiaowei He. 2026. A Nonlocal Unified Variational Framework for Free Surface Flows. In *Special Interest Group on Computer Graphics and Interactive Techniques Conference Conference Papers (SIGGRAPH Conference Papers '26), July 19–23, 2026, Los Angeles, CA, USA.* ACM, New York, NY, USA, 12 pages. https://doi.org/10.1145/3799902.3811196

1 Introduction

Free-surface flow is a common fluid dynamic phenomenon in nature. The dynamics of most free-surface flows are governed by three key physical mechanisms: incompressibility, viscosity, and surface tension. Consequently, accurate numerical simulation of such flows critically depends on the proper modeling and computation of these mechanisms. Recent advancements in implicit formulations for incompressibility [Bender and Koschier 2016] and viscosity [Weiler et al. 2018] have significantly enhanced the stability of fluid simulations. However, these solvers typically treat the governing physical mechanisms in a sequential and decoupled manner [Holz et al. 2025; Koschier et al. 2022]. This decoupled approach inevitably introduces splitting errors across the individual solution steps (as shown in Figure 2), which may compromise simulation stability and visual fidelity, especially with large time steps [Peer and Teschner 2016].

To mitigate splitting artifacts, several strategies have been developed. Larionov et al. [2017] proposed a unified variational framework for viscous and pressure terms from an Eulerian perspective, yielding a unified linear system free of coupling errors. However, this formulation is difficult to extend to particle-based methods due to

their unstructured, dynamic neighborhoods. Liu et al. [2022] adapted the SIMPLE algorithm [Patankar 2018] for SPH, coupling viscosity and pressure iteratively. While improving accuracy for viscous fluids, this approach requires multiple linear solves per time step, incurring substantial cost. Jeske et al. [2023] later coupled surface tension implicitly with viscosity, and Probst and Teschner [2024] proposed an LCP framework coupling IISPH and surface tension solvers, both markedly improving numerical stability.

Despite the progress outlined above, a unified treatment that fully accounts for the interdependence among incompressibility, viscosity, and surface tension remains an open problem. Fundamentally, fluid motion governed by the coupled effects of incompressibility, viscosity, and surface tension exhibits inherently nonlinear behavior. Consequently, the governing equations cannot be easily cast into a single linear system amenable to direct solution by a standard linear solver. Furthermore, the mathematical structures of these mechanisms are inherently heterogeneous: incompressibility imposes a global divergence-free (or constant-density) constraint, viscosity involves second-order derivatives of the velocity field, and surface tension arises from curvature-dependent interfacial forces. This disparity poses significant challenges for their unified modeling within a single computational framework.

In this work, we present a unified nonlinear optimization framework designed to achieve strong, unified coupling among incompressibility, viscosity, and surface tension. Our approach leverages peridynamics, a nonlocal continuum method naturally suited for multiphysics modeling, to provide a consistent mathematical basis for modeling these diverse fluid mechanisms. By following a variational principle, we cast the governing equations of fluid motion into a position-based nonlinear optimization problem. Our primary contribution lies in the incremental position-based formulation of viscosity, which seamlessly integrates viscous dissipation into a unified optimization framework alongside incompressibility and surface tension. The variational system is solved via the Semi-Implicit Successive Substitution Method (SISSM) [Lu et al. 2023], ensuring robust convergence and GPU-friendly parallelism. Thanks to a unified solver strategy, our method is capable of simulating a wide range of fluids stably: from low viscosity and high viscosity fluids to those with strong surface tension. For viscous fluids, our approach significantly enhances sharp surface details and improves morphological stability; for surface-tension-driven scenarios, it maintains stability even under extreme physical parameters. Furthermore, the framework incorporates separate treatments for bulk and shear viscosity, allowing for more refined control of different viscous fluid behaviors.

To the best of our knowledge, this is the first unified particle-based solver that unifies incompressibility, viscosity, and surface tension of free surface flows. Moreover, our method is straightforward to implement (as shown in Algorithm 1), it only requires iteratively solving a single equation that simultaneously enforces incompressibility, viscosity, and surface tension, yielding highly robust multiphysics fluid simulations. The main contributions of this work are summarized as follows:

- **A unified variational framework** for free-surface flows that enables a unified, nonlinear treatment of incompressibility, viscosity, and surface tension, effectively eliminating the splitting artifacts inherent in conventional multi-step solvers.
- **A position-based nonlocal viscosity solver**, which enables a more efficient and straightforward nonlinear coupling between viscous force and constant-density constraint;
- **A separate treatment of normal and shear viscous terms**, which allows finer control over viscous fluid behaviors.

2 Related Works

2.1 Incompressibility

Particle-based incompressibility is typically enforced via velocity-based or position-based constraints.

2.1.1 Velocity-based. methods derive pressure forces from the Navier-Stokes momentum equation to correct velocities. Explicit pressure methods, such as WCSPH [Becker and Teschner 2007; Desbrun and Gascuel 1996], are simple but prone to instability; Implicit iterative approaches [Bender and Koschier 2016; Bodin et al. 2011; He et al. 2012; Kang and Sagong 2014; Solenthaler and Pajarola 2009], and pressure Poisson equation methods [Ihmsen et al. 2013; Takahashi et al. 2018] offer markedly improved stability for large time steps. Dual-particle methods [Liu et al. 2025, 2024] further weaken the tension instability.

2.1.2 Position-based. methods avoid pressure solvers by enforcing density constraints directly on positions. PBF method [Macklin and Müller 2013] adapts the PBD framework [Macklin et al. 2016] to fluids; While SISPH [He et al. 2025] and IPBF [Diaz et al. 2025] reformulate incompressibility as a variational energy optimization to enhance the robustness and efficiency of fluid simulation. Besides the aforementioned SPH methods, the power particle method [De Goes et al. 2015] also uses a variational manner to enforce density constraints, and it incorporates well-shaped power diagrams for particle volume estimation, achieving excellent accuracy in incompressibility computation. This strategy has been extended to the PIC method [Qu et al. 2022] recently.

2.2 Viscosity

Since viscous stress is governed by the rate-of-deformation tensor, the majority of viscosity solvers are implemented based on velocity in particle methods. For low viscosity fluid simulations, particle methods often employ artificial viscosity [Schechter and Bridson 2012] to improve stability. For highly viscous fluids, early viscosity methods were mostly based on the explicit form of the shear stress momentum equation of fluids [de Souza Andrade et al. 2015; Müller et al. 2003], which suffered from poor stability. Therefore, various implicit viscous algorithms have been proposed, including implicit solvers with accurate shear stress discretization [Takahashi et al. 2015], and projection methods that damp specific components of the velocity gradient [Bender and Koschier 2016; Peer et al. 2015; Peer and Teschner 2016]. The state of the art of implicit viscosity mainly refers to the approach based on the improved discretization of the Laplacian of velocity [Weiler et al. 2018]. This method significantly enhances the accuracy of highly viscous fluid simulations

and achieves stable coiling and buckling effects. Subsequently, the improved implicit viscosity method [Weiler et al. 2018] is extended to the simulation of non-Newtonian fluids [Liu et al. 2022; Zhang et al. 2024], which exhibit variable viscosity that depends on strain rate or other physical factors.

2.3 Surface tension

Surface tension arises from intermolecular attractive forces between microscopic fluid molecules. For a particle near the free surface, the net attractive force points inward, producing a surface tension effect that acts to minimize surface area [Berry 1971]. Numerically, surface tension can be modeled in two main ways: the macroscopic methods that apply curvature-derived body forces or minimize the fluid surface area; and the microscopic methods that apply pairwise forces between particles. Among macroscopic approaches, the Continuum Surface Force (CSF) method is a well-established technique [Adami et al. 2010; Müller et al. 2003]. To achieve greater robustness, the method based on the free surface energy functional within the diffuse interface model has been proposed [He et al. 2014]. In recent research, this free surface energy-based method has been extended to simulate adsorption and friction between fluids and solids [Probst and Teschner 2024]. In contrast, microscopic pairwise-force models assume short-range attractive forces between neighboring particles [Akinci et al. 2013]. These methods not only reproduce surface tension effects at the free surface, but also naturally handle fluid–solid adhesion and complex multiphase phenomena such as immiscible fluid mixing [Yang et al. 2017]. To further improve the stability of this method, an implicit pairwise force formulation has recently been proposed [Jeske et al. 2023], enabling more accurate simulation of high-strength surface tension.

2.4 Coupling of solvers

Coupling errors between different solution steps are common in various areas of physical simulation, such as fluid–solid interaction [Abu Rumman et al. 2020; Gissler et al. 2019; Probst and Teschner 2023]. However, the mutual interference between different physical mechanisms within the fluid itself, such as incompressibility, viscosity, and surface tension, has received comparatively little attention in the computer graphics community. In Eulerian methods, the structured spatial grid facilitates the development of unified solvers. Notably, variational energy frameworks have been optimized to construct monolithic linear systems that simultaneously account for viscosity and incompressibility [Goldade et al. 2019; Larionov et al. 2017], These unified Eulerian approaches can vividly capture complex behaviors of highly viscous fluids. In particle-based methods, SIMPLE (Semi Implicit Method for Pressure Linked Equation) iterative method [Patankar 2018] was introduced to couple the implicit viscosity and pressure solvers [Liu et al. 2022], which alternately solves implicit pressure and viscosity systems to reduce their mutual interference. This method can stably simulate the high viscosity fluids with sharp features. Recently, an implicit unified solver for surface tension and viscosity has been proposed [Jeske et al. 2023], enabling more accurate simulation of fluids with large surface tension. Probst and Teschner [2024] unified IISPH [Ihmsen et al. 2013], surface tension, and fluid–solid adhesion in a single LCP-based framework, enabling stable and accurate simulation of wetting phenomena on solid boundaries.

3 Background

Peridynamics [Silling 2000; Silling et al. 2007] reformulates continuum mechanics by replacing partial differential equations with a non-local integral form, making it particularly well-suited for modeling multi-physics phenomena [He et al. 2017; Yan and Ren 2023]. As our approach is grounded in peridynamics, we first provide a brief overview of the relevant background theory before presenting our method.

In peridynamics, the continuous body is discretized into material points. The state of a material point i is influenced by other points j within a finite distance, known as its horizon $\mathcal{H}$. For a particle whose initial position is $\mathbf{x}_i$ and its neighborhood particle is $\mathbf{x}_j$, the relative position in the reference between i and j is $\xi_{ij} = \mathbf{x}_{ij} = \mathbf{x}_j - \mathbf{x}_i \in \mathcal{H}$, which is named as **bond**. When a material undergoes deformation, the relative positions of particles will change to $\mathbf{y}$, and the corresponding deformation vector state is $\mathbf{y}_{ij} = \mathbf{y}_j - \mathbf{y}_i$. Accordingly, the deformation gradient tensor of particle i in the state-based peridynamics [He et al. 2017; Wang et al. 2025] is:

$$\mathbf{F}_i = \left(\sum_j w_{ij} (\mathbf{y}_{ij} \otimes \xi_{ij}) V_j \right) \cdot \mathbf{K}_i^{-1}, \quad \mathbf{K}_i = \sum_j w_{ij} \xi_{ij} \otimes \xi_{ij} V_j. \quad (1)$$

Here the w_{ij} is the kernel function for ξ_{ij}, V_j is the volume of particle j, and the $\mathbf{K}$ is named as the shape tensor [Silling et al. 2007]. The linear momentum balance in state-based peridynamics is governed by an integral equation:

$$\rho_i \dot{\mathbf{v}}_i = \sum_j (\underline{\mathbf{T}}_i \langle \xi_{ij} \rangle - \underline{\mathbf{T}}_j \langle \xi_{ji} \rangle) V_j \,, \quad (2)$$

where ρ_i is density of particle i, and $\underline{\mathbf{T}}$ is the force vector state, which can be constructed from the first Piola–Kirchhoff stress $\mathbf{P}$ via the following equation: $\underline{\mathbf{T}}_i \langle \xi_{ij} \rangle = w_{ij} \mathbf{P}_i \cdot \mathbf{K}_i^{-1} \cdot \xi_{ij}$.

However, applying the aforementioned state-based force state $\underline{\mathbf{T}}$ to fluids poses significant numerical challenges. Specifically, the disordered particle distributions inherent in fluid motion often lead to a singular shape tensor $\mathbf{K}$, causing numerical instabilities. Therefore, we adopt a bond-based assumption to simplify the computation of force state $\underline{\mathbf{T}}_i \langle \xi_{ij} \rangle$. Following previous works [Silling et al. 2007; Zhao et al. 2022], we assume that interaction force $\underline{\mathbf{T}}_i \langle \xi_{ij} \rangle$ between two particles, i.e., i and j, depends solely on the relative deformation of the bond itself (ξ_{ij}), independent of the collective neighborhood state. The nonlocal pairwise forces $\underline{\mathbf{T}}_{ij}$ for incompressibility, surface tension, and viscosity will be detailed in the next section.

4 Model

To achieve strong coupling among different physical mechanisms, the variational energy framework offers a highly suitable approach. In this framework, individual mechanical effects are formulated as potential energy terms, and their coupling is naturally enforced through energy minimization derived from the variational principle [Daviet et al. 2025; Giles et al. 2025; Huang et al. 2025]. From the perspective of variational energy principles, the motion of meshfree particle-based fluids incorporating incompressibility, viscosity,

and surface tension can be formulated as an energy minimization problem:

$$\mathbf{y} = \arg\min_{\mathbf{y}} E(\mathbf{y}) \,, \tag{3}$$

where total incremental potential $E(\mathbf{y})$ is defined as:

$$E(\mathbf{y}) = \frac{m}{2h^2} \left\| \mathbf{y} - \mathbf{y}^* \right\|_2^2 + \Phi(\mathbf{y}) + \Psi(\mathbf{y}) + \Upsilon(\mathbf{y}), \tag{4}$$

where i is the index of fluid particle, $\mathbf{y}^*$ is the particle position updated via the intermediate velocity $\mathbf{v}^*$:

$$\mathbf{y}^* = \mathbf{x} + h \cdot \mathbf{v}^*, \tag{5}$$

and m is particle mass. Here, $\Phi(\mathbf{y})$ is bulk potential of fluid to enforce incompressibility, $\Psi(\mathbf{y})$ is incremental potential for viscous dissipation to model viscosity, and $\Upsilon(\mathbf{y})$ is the incremental potential for surface tension, which are all defined as functions of the deformed particle position vector $\mathbf{y}$.

Solving this variational problem (Equation 3) yields the updated particle positions [Fernández-Fernández et al. 2025; Lu and Hu 2025], which implicitly account for the combined effects of incompressibility, viscosity, and surface tension. In the following subsections, we will leverage non-local theory and draw upon existing approaches to develop these potential energy terms for free-surface flows.

4.1 Incompressibility

Incompressibility refers to the constraint of constant volume during deformation, i.e., the constant density constraint in fluids. It also arises in the modeling of elastic solids. Following the Neo-Hookean hyperelastic model of elastic solids [Smith et al. 2018], the potential associated with resistance to volumetric deformation can be expressed as a function of the volume ratio J:

$$\Phi = \frac{\kappa}{2}(J-1)^2, \tag{6}$$

where J is defined as $J = \det(\mathbf{F})$. In modeling incompressible fluids, the volumetric response is assumed isotropic. Thus, the volume ratio J_i of fluid particle i can be approximated by the relative density: $J_i = \frac{\rho_i}{\rho_0}$. Here, ρ_0 is the rest density of fluid, the density ρ_i can be computed as $\rho_i = \sum_j mW(|\mathbf{y}_{ij}|, \widetilde{h})$, W is the SPH kernel function, and $\widetilde{h}$ is the smoothing length in SPH method [Koschier et al. 2020]. As such, the incompressibility-related potential for free surface flows, i.e., the bulk energy term, is defined as:

$$\Phi(\mathbf{y}) = \frac{\kappa}{2} \sum_i (\frac{\rho_i}{\rho_0} - 1)^2, \tag{7}$$

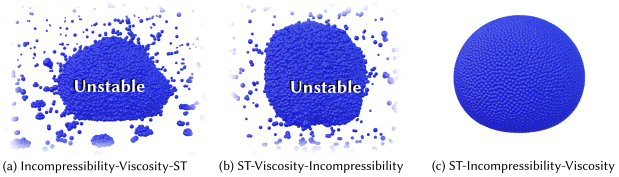

(a) Incompressibility-Viscosity-ST (b) ST-Viscosity-Incompressibility (c) ST-Incompressibility-Viscosity

Fig. 2. For fluids with strong surface tension, the order of solving steps significantly affects the stability of simulation. (a) Incompressibility → Viscosity → Surface Tension; (b) Surface Tension → Viscosity → Incompressibility; (c) Surface Tension → Incompressibility → Viscosity.

which is very similar to [Diaz et al. 2025; He et al. 2025]. Accordingly, the variational derivative of the bulk energy term $\Phi_i(\mathbf{y})$ is given by:

$$\frac{\partial \Phi(\mathbf{y})}{\partial \mathbf{y}_i} = \sum_j \left\{ \tilde{\mathbf{T}}_{ji}^p - \tilde{\mathbf{T}}_{ij}^p \right\} \,, \tag{8}$$

where $\tilde{\mathbf{T}}_{ij}^p = \kappa(J_i - 1)\frac{m w(|\mathbf{y}_{ij}|)}{\rho_0}\mathbf{I} \cdot \frac{\mathbf{y}_{ij}}{|\mathbf{y}_{ij}|}$. Here κ is the constant coefficient which determines the strength of incompressibility; J_i is calculated as $J_i = \frac{\rho_i}{\rho_0}$; $\mathbf{I}$ denotes the identity matrix. w represents the first derivative of SPH kernel function W, i.e., $w(|\mathbf{y}_{ij}|) = \dot{W}(|\mathbf{y}_{ij}|, \widetilde{h}) \leq 0$.

Although the above bulk energy for fluids is inspired by the Neo-Hookean hyperelastic model for solids, the model is numerically equivalent to the SISPH method [He et al. 2025].

4.2 Viscosity

To achieve a strong coupling between viscosity and the position-based bulk constraint (incompressibility), the primary challenge lies in the disparate nature of their classical formulations. To bridge this gap, we depart from the traditional velocity-based Laplacian approach [Weiler et al. 2018] and introduce the following approach. First, we reformulate viscous dissipation as a nonlocal incremental potential, ensuring variational consistency with other physical mechanisms. Second, by embedding the kinematic relationship between velocity and position directly into this potential, we propose a position-based viscosity model.

4.2.1 Nonlocal incremental potential for viscosity. In continuum mechanics, the classic viscous dissipation function [Batchelor 1967; White and Majdalani 2006] is given by the following expression:

$$\Psi(\dot{\varepsilon}) = \frac{1}{2}\left\{ \mu \mathbf{tr}(\dot{\varepsilon}^2) + \frac{\lambda}{2}\mathbf{tr}(\dot{\varepsilon})^2 \right\} \,, \tag{9}$$

which closely resembles that of the linear elastic model characterized by Lamé constants [Lai et al. 2009], where λ is the viscosity coefficient of volumetric strain rate, μ is the viscosity coefficient for shear strain rate, and $\dot{\varepsilon}$ is the rate of strain tensor ($\dot{\varepsilon} = \frac{1}{2}(\nabla\mathbf{v} + \nabla\mathbf{v}^T)$). For ideal incompressible fluids, the bulk viscosity term is typically negligible due to the velocity-divergence-free condition ($\nabla \cdot \mathbf{v} = 0$) [Weiler et al. 2018]. However, in most particle-based fluid simulation methods, a positive velocity divergence is permitted ($\nabla \cdot \mathbf{v} > 0$), due to the negative pressures clamping approach to avoid instability [Koschier et al. 2020, 2022]. It renders bulk viscosity non-negligible.

To model this viscous dissipation within a non-local framework, we begin by analyzing two distinct modes of inter-particle deformation. For the bond of particles i and j, the deformation comprises a normal component along the bond (connecting line of particle i and j), i.e.,ϵ_{ij}, and a tangential component perpendicular to the bond, i.e., Δ_{ij}. Inspired by previous peridynamics works [Zhao et al. 2022; Zhu and Ni 2017], we define the normal deformation ϵ_{ij} and tangential deformation Δ_{ij} between particles i and j as follows:

$$\epsilon_{ij} = (\mathbf{v}_{ij} \cdot \mathbf{n}_{ij})\mathbf{n}_{ij} \,,$$
$$\Delta_{ij} = \mathbf{v}_{ij} - (\mathbf{v}_{ij} \cdot \mathbf{n}_{ij})\mathbf{n}_{ij} \,.$$

where $\mathbf{v}_{ij} = \mathbf{v}_j - \mathbf{v}_i$, $\mathbf{n}_{ij}$ is the unit normal vector along the line connecting the particle i and j, i.e., $\mathbf{n}_{ij} = \frac{\mathbf{x}_{ij}}{|\mathbf{x}_{ij}|}$. Accordingly, we

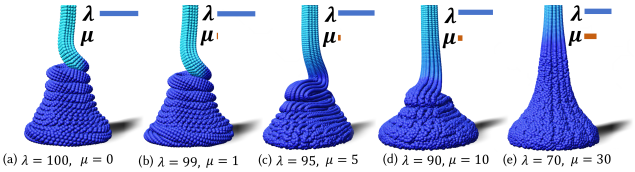

Fig. 3. Coiling of viscous fluids under varying bulk (λ) and shear (μ) viscosities. Our method accurately captures the coiling dynamics. Increasing shear viscosity significantly suppresses the coiling effect.

reformulate the continuum expression for viscous dissipation (Equation 9) as a nonlocal incremental potential energy defined over particle velocities:

$$\Psi(\mathbf{v}) = \frac{m}{\rho_0}\sum_i\left\{\sum_j(\frac{\mu}{2}\left|\Delta_{ij}\right|^2+\frac{\lambda}{4}\left|\epsilon_{ij}\right|^2)\omega(|\mathbf{x}_{ij}|)\right\}. \tag{10}$$

Here, the weight function ω is defined as $\omega(|\mathbf{x}_{ij}|) = -w(|\mathbf{x}_{ij}|) = -\dot{W}(|\mathbf{x}_{ij}|, \widetilde{h})$. In the above viscous model, the strengths of bulk and shear viscosities are controlled independently by the parameters λ and μ, respectively. This enables more precise control over the behavior of viscous fluids, as illustrated in Figure 3.

4.2.2 Position-based viscosity. To integrate the incremental viscous potential (Equation 10) into a position-based framework, we replace particle velocities with position increments via:

$$\mathbf{v}_{ij} = \frac{\mathbf{y}_{ij}-\mathbf{x}_{ij}}{h}. \tag{11}$$

By inserting this formula into Equation 10, the velocity-based dissipation is transformed into a position-based incremental potential $\Psi(\mathbf{y})$. Taking the gradient of this potential with respect to the particle positions gives:

$$\frac{\partial\Psi(\mathbf{y})}{\partial\mathbf{y}_i} = \sum_j\left\{\tilde{\mathbf{T}}^v_{ji}-\tilde{\mathbf{T}}^v_{ij}\right\}, \tag{12}$$

where $\tilde{\mathbf{T}}^v_{ij}(\mathbf{y}) = -(\lambda\Lambda_{ij}+\mu\mathbf{M}_{ij})\cdot\left(\mathbf{y}_{ij}-\mathbf{x}_{ij}\right)$, the matrix Λ_{ij} and $\mathbf{M}_{ij}$ are:

$$\Lambda_{ij} = \frac{mw(|\mathbf{x}_{ij}|)}{2h\rho_0}(\mathbf{n}_{ij}\mathbf{n}_{ij});\ \mathbf{M}_{ij} = \frac{mw(|\mathbf{x}_{ij}|)}{h\rho_0}(\mathbf{I}-\mathbf{n}_{ij}\mathbf{n}_{ij}). \tag{13}$$

4.3 Surface tension

Following microscopic surface tension modeling methods [Akinci et al. 2013; Jeske et al. 2023; Yang et al. 2017], the surface tension of a fluid arises from intermolecular attractive forces, which are conceptually similar to the long-range, pairwise-defined interactions in peridynamics. Accordingly, a microscopic surface tension can be formulated such that its potential energy rises with interparticle distance, which is minimized when the distance equals the initial equilibrium spacing (Figure 4(a)). The intermolecular interaction potential energy between particles i and j is denoted by the function $C(|\mathbf{y}_{ij}|)$. As such, the total surface tension of particle i is then given

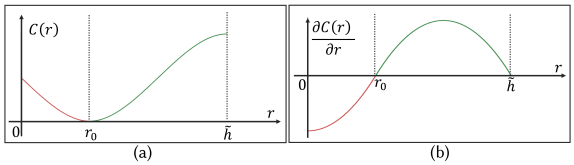

Fig. 4. Pairwise potential energy for surface tension (a) and its first derivative with respect to inter-particle distance (b). $\widetilde{h}$ is the radius of neighborhood. Similar to van der Waals interactions, particles experience repulsion at short ranges (red region of the potential curve) to resist compression and attraction at longer ranges (green region). The potential energy is minimized when the interparticle distance matches the equilibrium spacing (r_0).

by the following expression:

$$\Upsilon(\mathbf{y}) = \gamma m^2\sum_i\left\{\sum_j C(|\mathbf{y}_{ij}|)\right\} \tag{14}$$

where the profile of $C(|\mathbf{y}_{ij}|)$ is illustrated in Figure 4.

Taking the variational derivative of the total interparticle potential energy in Equation 14, yields the surface tension equation for the particles, which takes the same form as the discretized Equation 2:

$$\frac{\partial\Upsilon(\mathbf{y})}{\partial\mathbf{y}_i} = \sum_j\left\{\tilde{\mathbf{T}}^{st}_{ji}-\tilde{\mathbf{T}}^{st}_{ij}\right\}. \tag{15}$$

where $\tilde{\mathbf{T}}^{st}_{ij} = \gamma m^2 c(|\mathbf{y}_{ij}|)\cdot\mathbf{I}\cdot\frac{\mathbf{y}_{ij}}{|\mathbf{y}_{ij}|}$. Here γ is a parameter to determine the strength of the surface tension effect, and $c(r)$ is the scalar kernel function of the inter-particle distance, which is the derivative of the C, i.e., $c(r) = \frac{\partial C(r)}{\partial r}$. In particular, although the derivation stems from a unified variational principle, the resulting $\tilde{\mathbf{T}}^{st}_{ij}$ is formally equivalent to the pairwise models devised by [Akinci et al. 2013; Tartakovsky and Meakin 2005; Yang et al. 2017], which exhibit the same interparticle interaction characteristics as illustrated in Figure 4(b). Therefore, the spline kernel function of the pairwise force from such models, i.e. $c(r)$, can be directly employed to compute the surface tension force state $\tilde{\mathbf{T}}^{st}_{ij}$.

5 Unified solver

Following the formulation of a unified variational optimization model for free-surface flows, the choice of an efficient nonlinear solver becomes essential. Conventional approaches like the Newton method generally involve second-order derivatives of the variational functional, leading to implementation complexity. Therefore, we

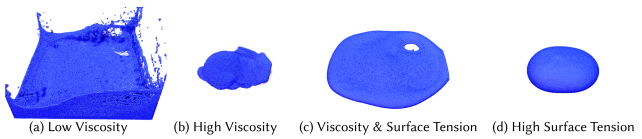

Fig. 5. Different fluids. (a) Low viscosity fluid ($\kappa = 1, \lambda = 0.2, \mu = 0.01, \gamma = 0.01$); (b) High viscosity fluid ($\kappa = 1, \lambda = 200, \mu = 1, \gamma = 0.01$); (c) Fluid with moderate viscosity and surface tension ($\kappa = 1, \lambda = 40, \mu = 1, \gamma = 200$); (d) High surface tension fluid ($\kappa = 1, \lambda = 0.2, \mu = 0.01, \gamma = 1000$).

adopt the Semi-implicit Successive Substitution Method (SISSM) [Lu et al. 2023], a simple, easily parallelizable nonlinear optimization approach that avoids second-order differentiation.

5.1 Optimization of the unified variational fluid model

As an extension of the fixed-point iteration method, our semi-implicit iteration approach is designed to solve the nonlinear system by reformulating it into a convergent iterative scheme:

$$\mathbf{y}^{k+1} = g(\mathbf{y}^k)\,, \tag{16}$$

and k means the iteration number. The iteration will converge if the following criteria are satisfied: $|g'(\mathbf{y})| < 1$. To handle cases where the above convergence criteria are violated, we follow Lu et al. [2023], and reformulate the fixed-point iteration Equation 16 in a semi-implicit manner to guarantee the convergence. The modified scheme is given by:

$$\mathbf{y}^{k+1} = f^{+}(\mathbf{y}^k)(\tilde{\mathbf{y}}^k - \mathbf{y}^{k+1}) + f^{-}(\mathbf{y}^k)(\tilde{\mathbf{y}}^k - \mathbf{y}^k) + \mathbf{b}\,. \tag{17}$$

Here, $\tilde{\mathbf{y}}$ represents the positions of neighboring particles of $\mathbf{y}$, $\mathbf{b}$ is a constant vector independent of $\mathbf{y}$. The coefficient function $f^{+}(\mathbf{y})$ is constructed to be strictly non-negative, and $f^{-}(\mathbf{y})$ is non-positive. Consequently, the semi-implicit iteration is reformulated to guarantee convergence as follows:

$$\mathbf{y}^{k+1} = \frac{f^{+}(\mathbf{y}^k)\tilde{\mathbf{y}}^k + f^{-}(\mathbf{y}^k)(\tilde{\mathbf{y}}^k - \mathbf{y}^k) + \mathbf{b}}{1 + f^{+}(\mathbf{y}^k)}\,. \tag{18}$$

Next, we apply this semi-implicit scheme to optimize our variational energy model (Equation 3).

Taking the variational derivative of the total energy (Equation 3) and simplifying, we obtain the following equation:

$$\mathbf{y}_i = \mathbf{y}_i^* + \frac{h^2}{m}\sum_j \left\{\tilde{\mathbf{T}}_{ij}^{p} + \tilde{\mathbf{T}}_{ij}^{v} + \tilde{\mathbf{T}}_{ij}^{st}\right\}. \tag{19}$$

Here the $\tilde{\mathbf{T}}_{ij}^{p}$, $\tilde{\mathbf{T}}_{ij}^{v}$ and $\tilde{\mathbf{T}}_{ij}^{st}$ are functions of the particle position $\mathbf{y}$ (Equation 8, 12 and 15). For notational simplicity, we initially present only the force state $\tilde{\mathbf{T}}_{ij}$ acting on particle i from neighbor j, omitting the $\tilde{\mathbf{T}}_{ji}$. Following the strategy in Equation 18, we decompose each force state term ($\tilde{\mathbf{T}}_{ij}^{p}, \tilde{\mathbf{T}}_{ij}^{v}, \tilde{\mathbf{T}}_{ij}^{st}$) into semi-implicit components:

5.1.1 Force state for incompressibility. ($\tilde{\mathbf{T}}_{ij}^{p}$): As our bulk potential model (Equation 8) is exactly identical to that in SISPH [He et al. 2025], we directly adopt its established splitting strategy:

$$\tilde{\mathbf{T}}_{ij}^{p} = \hat{\mathbf{T}}_{ij}^{p+}\cdot(\mathbf{y}_j^k - \mathbf{y}_i^{k+1}) + \hat{\mathbf{T}}_{ij}^{p-}\cdot(\mathbf{y}_j^k - \mathbf{y}_i^k)\,, \tag{20}$$

where $\hat{\mathbf{T}}_{ij}^{p+} = -\kappa\frac{m}{\rho_0}\frac{w(|\mathbf{y}_{ij}|)}{|\mathbf{y}_{ij}|}\mathbf{I}$ and $\hat{\mathbf{T}}_{ij}^{p-} = \kappa\frac{m}{\rho_0}J_i\frac{w(|\mathbf{y}_{ij}|)}{|\mathbf{y}_{ij}|}\mathbf{I}$. Here w is the first differential of SPH kernel function W, which is strictly non-positive, i.e., $w(r) \le 0$.

5.1.2 Force state for viscosity. ($\tilde{\mathbf{T}}_{ij}^{v}$): Our viscosity model based on the position-based incremental potential (Equation 12) is naturally amenable to a semi-implicit iterative formulation:

$$\tilde{\mathbf{T}}_{ij}^{v} = \hat{\mathbf{T}}_{ij}^{v+}\cdot(\mathbf{y}_j^k - \mathbf{y}_i^{k+1}) - \hat{\mathbf{T}}_{ij}^{v+}\cdot(\mathbf{x}_j - \mathbf{x}_i)\,, \tag{21}$$

where $\hat{\mathbf{T}}_{ij}^{v+} = -(\lambda\Lambda_{ij} + \mu\mathbf{M}_{ij})$. Referring to Equation 13, as the matrix $\hat{\mathbf{T}}_{ij}^{v+}$ is generally positive definite or positive semi-definite, no explicit term $\hat{\mathbf{T}}_{ij}^{v-}$ is required.

5.1.3 Force state for surface tension. ($\tilde{\mathbf{T}}_{ij}^{st}$): The semi-implicit form of the incremental potential for surface tension is derived as:

$$\tilde{\mathbf{T}}_{ij}^{st} = \hat{\mathbf{T}}_{ij}^{st+}\cdot(\mathbf{y}_j^k - \mathbf{y}_i^{k+1}) + \hat{\mathbf{T}}_{ij}^{st-}\cdot(\mathbf{y}_j^k - \mathbf{y}_i^k)\,, \tag{22}$$

where $\hat{\mathbf{T}}_{ij}^{st+} = \gamma m^2\frac{c^{+}(|\mathbf{y}_{ij}|)}{|\mathbf{y}_{ij}|}\mathbf{I}$, and $\hat{\mathbf{T}}_{ij}^{st-} = \gamma m^2\frac{c^{-}(|\mathbf{y}_{ij}|)}{|\mathbf{y}_{ij}|}\mathbf{I}$. The division between $\hat{\mathbf{T}}_{ij}^{st+}$ and $\hat{\mathbf{T}}_{ij}^{st-}$ arises due to the pairwise kernel function c associated with surface tension. Since c is represented as a piecewise polynomial function [Akinci et al. 2013; Jeske et al. 2023], it can be conveniently decomposed into $c(r) = c^{+}(r) + c^{-}(r)$, with $c^{+}(r)$ representing the positive part of $c(r)$, and $c^{-}(r)$ representing the negative part.

After implementing the above modifications, the final semi-implicit iterative equation for particle positions, which incorporates incompressibility, viscosity, and surface tension, is given as follows:

$$\mathbf{y}_i^{k+1} = \mathbf{y}_i^* + \sum_j \left\{\mathbf{A}_{ij}^{+}\cdot(\mathbf{y}_j^k - \mathbf{y}_i^{k+1}) + \mathbf{A}_{ij}^{-}\cdot(\mathbf{y}_j^k - \mathbf{y}_i^k) - \mathbf{b}_{ij}\right\}, \tag{23}$$

where $\mathbf{y}_i^*$ is intermediate particle position (Equation 5), and $\mathbf{A}_{ij}^{+} = m^{-1}h^2(\hat{\mathbf{T}}_{ij}^{p+} + \hat{\mathbf{T}}_{ij}^{v+} + \hat{\mathbf{T}}_{ij}^{st+}), \mathbf{A}_{ij}^{-} = m^{-1}h^2(\hat{\mathbf{T}}_{ij}^{p-} + \hat{\mathbf{T}}_{ij}^{st-}), \mathbf{b}_{ij} = m^{-1}h^2\hat{\mathbf{T}}_{ij}^{v+}\cdot(\mathbf{x}_j - \mathbf{x}_i)$. Subsequently, particle positions $\mathbf{y}^{k+1}$ are updated via the semi-implicit iteration below, which unifies the treatment of viscosity, incompressibility, and surface tension within a single numerical framework:

$$\mathbf{y}_i^{k+1} = \left(\mathbf{I} + \sum_j \mathbf{A}_{ij}^{+}\right)^{-1}\cdot\left(\mathbf{y}_i^* + \sum_j\left(\mathbf{A}_{ij}^{+}\cdot\mathbf{y}_j^k + \mathbf{A}_{ij}^{-}\cdot\mathbf{y}_{ij}^k - \mathbf{b}_{ij}\right)\right). \tag{24}$$

Following the nonlocal momentum Equation 2 and the exact differential of the global variational energy, Equation 19 must incorporate the force state exerted by particle i on neighboring particle j, i.e., $\tilde{\mathbf{T}}_{ji}$, to guarantee global conservation of linear momentum:

$$\mathbf{y}_i = \mathbf{y}_i^* + \frac{h^2}{m}\sum_j\left\{\tilde{\mathbf{T}}_{ij}^{v} + \tilde{\mathbf{T}}_{ij}^{st} + \tilde{\mathbf{T}}_{ij}^{p} - \tilde{\mathbf{T}}_{ji}^{v} - \tilde{\mathbf{T}}_{ji}^{st} - \tilde{\mathbf{T}}_{ji}^{p}\right\}. \tag{25}$$

Consequently, the refined iterative equation for particle positions $\mathbf{y}^{k+1}$ is given by:

$$\mathbf{y}_i^{k+1} = \left(\mathbf{I} + \sum_j(\mathbf{A}_{ij}^{+} + \mathbf{A}_{ji}^{+})\right)^{-1}\cdot \left(\mathbf{y}_i^* + \sum_j\left((\mathbf{A}_{ij}^{+} + \mathbf{A}_{ji}^{+})\cdot\mathbf{y}_j^k + (\mathbf{A}_{ij}^{-} + \mathbf{A}_{ji}^{-})\cdot\mathbf{y}_{ij}^k - (\mathbf{b}_{ij} + \mathbf{b}_{ji})\right)\right). \tag{26}$$

The fixed-point iterative algorithm based on the above equation preserves linear momentum while consistently coupling the incompressibility, viscosity, and surface tension effect for particle position updates. It is worth noting that Equation 26 can be straightforwardly

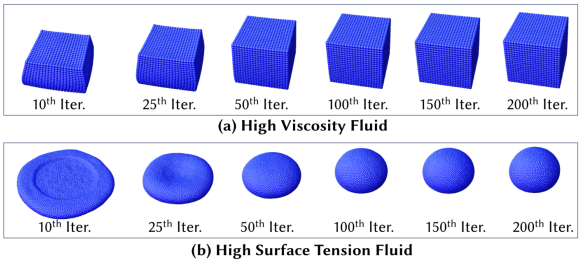

Fig. 6. Results for (a) a high-viscosity fluid and (b) a high-surface-tension fluid. Each fluid is simulated with a different fixed number of solver iterations. (a) $\kappa = 1, \lambda = 200, \mu = 0.1, \gamma = 1$; (b) $\kappa = 1, \lambda = 2, \mu = 0.1, \gamma = 1000$.

implemented in a GPU-parallelized setting by extending the code for Equation 24 with atomic operations. For instance, if we aim to calculate $\mathbf{A}_i^+ = \sum_j (\mathbf{A}_{ij}^+ + \mathbf{A}_{ji}^+)$, during the accumulation of $\mathbf{A}_{ij}^+$ to $\mathbf{A}_i^+$ on thread i, the same value $\mathbf{A}_{ij}^+$ can be atomically added in reverse to $\mathbf{A}_j^+$ on thread j.

5.2 Convergence analysis

We assess the convergence of the semi-implicit iterative solver (Equation 26) by simulating a high-viscosity fluid and a high surface tension fluid with increasing fixed iteration counts. As shown in Figure 6, the fluid shapes stabilize progressively. Beyond 100 iterations, no perceptible difference can be observed, the results indicate the convergence of the iterative solver.

We further analyze the convergence behavior using the test scenarios from Figure 6. We adopt the relative error estimation approach for SISSM proposed by He et al. [2025], with the resulting convergence curve shown in Figure 7(a):

$$\epsilon^k = \frac{E\left(\mathbf{y}^k\right) - E\left(\mathbf{y}^N\right)}{E\left(\mathbf{y}^0\right) - E\left(\mathbf{y}^N\right)}, \tag{27}$$

where $\mathbf{y}^0$ is the initial guess of particle position, $\mathbf{y}^k$ is the k-th iterate particle position, $\mathbf{y}^N$ is the final iterate particle position. In our test, N is set to 200. Additionally, we directly compute the update of particle positions between consecutive iterations and plot their

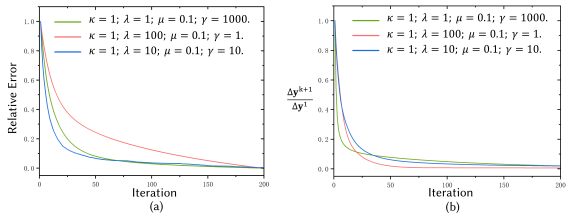

Fig. 7. Convergence curves of the unified variational solver based on the SISSM method, evaluated on the scenarios shown in Figure 6. (a) Convergence measured using the relative error in Equation 27; (b) Convergence measured using the position update norm in Equation 28.

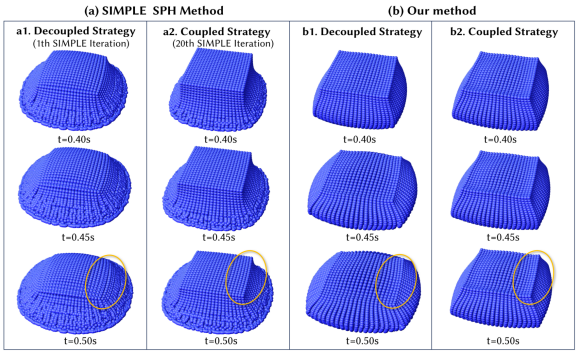

Fig. 8. Viscosity fluids. (a1) SIMPLE SPH method [Liu et al. 2022] with a single SIMPLE iteration, decoupling viscosity [Weiler et al. 2018] and incompressibility [Kang and Sagong 2014]; (a2) SIMPLE SPH method [Liu et al. 2022] with 20 SIMPLE iterations to couple viscosity and incompressibility; (b1) Our semi-implicit variational method with decoupled treatment of viscosity and incompressibility; (b2) Our unified method with strong coupling between viscosity and incompressibility.

evolution in Figure 7(b):

$$\frac{\Delta \mathbf{y}^{k+1}}{\Delta \mathbf{y}^1} = \frac{\left|\mathbf{y}^{k+1} - \mathbf{y}^k\right|}{\left|\mathbf{y}^1 - \mathbf{y}^0\right|}. \tag{28}$$

These results demonstrate that our unified solver converges effectively.

6 Validation and Discussion

All experiments were performed on a computer equipped with an Intel i9-12800K processor running at 2.90 GHz, an NVIDIA GeForce RTX 4080 Super GPU, and 32GB RAM. To ensure high efficiency, all components—including neighbor search, the unified physics solver for incompressibility, viscosity, and surface tension—are fully parallelized on the GPU, the algorithm is as shown in Algorithm 1. Solid boundaries are represented by ghost particles [Akinci et al. 2012] or Signed-distance fields [Ren et al. 2023; Zhang et al. 2025]. Performance metrics for large-scale simulations are reported in Table 1. In all test scenarios of this paper, the kernel function W is

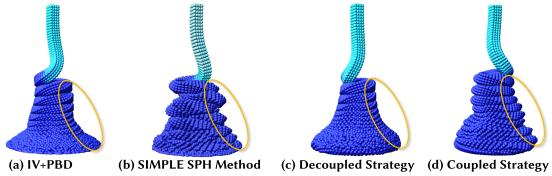

Fig. 9. Coiling effects of viscous fluids. (a) Implicit viscosity [Weiler et al. 2018] combined with PBF [Macklin and Müller 2013]; (b) SIMPLE SPH method [Liu et al. 2022] with 5 SIMPLE iterations to couple viscosity [Weiler et al. 2018] and incompressibility [Nair and Tomar 2014]; (c) Our semi-implicit variational method with decoupled treatment of viscosity and incompressibility; (d) Our unified method with strong coupling between viscosity and incompressibility.

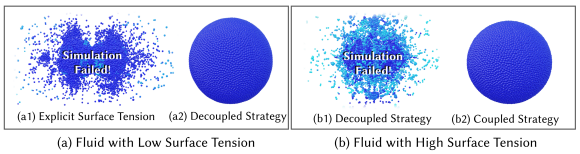

Fig. 10. Coalescence of two cubic fluid blobs into a single sphere under different surface tension treatments. (a1) Explicit surface tension; (a2) Our semi-implicit variational method with decoupled treatment, $\gamma = 500$; (b1) Our semi-implicit variational method with decoupled treatment, $\gamma = 2000$; (b2) Our unified variational method coupling incompressibility, viscosity, and surface tension, $\gamma = 2000$.

spiky kernel in [Müller et al. 2003], and the function c in surface tension model is the pairwise force function in [Akinci et al. 2013].

6.1 Decoupled and coupled strategies

To validate the effectiveness of our proposed unified method, we conduct comparisons between the decoupled strategy and coupled strategy (i.e., our unified method). The decoupled variant of our algorithm is implemented by setting the parameters for incompressibility, viscosity, and surface tension to zero, respectively, and then applying the solver sequentially (once per effect) in a prescribed order, effectively reproducing an operator-splitting scheme.

6.1.1 Conflicts among different solving steps. To demonstrate the coupling conflict among surface tension, incompressibility, and viscosity, we combine three independent solvers—namely, an incompressibility solver, a viscosity solver, and a pairwise surface tension solver—to simulate a fluid with a very large surface-tension coefficient. As shown in Figure 2, the order in which these solvers are applied within a single time step critically affects stability: only the sequence "surface tension → incompressibility → viscosity" yields a stable simulation.

6.1.2 Comparison of high viscous fluids. To demonstrate the effectiveness of our strongly coupling strategy for incompressibility and viscosity, we simulate a highly viscous fluid using different approaches. As shown in Figure 8, in the SPH-based SIMPLE algorithm [Liu et al. 2022], the fluid rapidly collapses when the decoupled strategy is used (SIMPLE iteration count is set to 1), whereas with a coupled strategy (20 SIMPLE iterations), the shape of the fluid remains stable and its sharp corners are preserved. A similar trend is

Fig. 11. Surface-tension-dominated fluids (velocities are color-coded). (a) Decoupled treatment of surface tension, viscosity, and incompressibility leads to numerical instability. (b) Our unified method with strong coupling of all three effects ensures stable and robust simulation.

Fig. 12. Melted sugar and pitch (50k particles per fluid). The melted sugar is modeled with high bulk viscosity ($\lambda = 400$) and low shear viscosity ($\mu = 0.1$), producing clear buckling and coiling; the pitch is assigned lower bulk viscosity ($\lambda = 300$) and higher shear viscosity ($\mu = 100$), which suppresses the buckling and coiling effects.

observed with our method: the decoupled variant leads to instability, while the unified incompressibility–viscosity solver maintains the stable shape and fine geometric features of the fluid cube.

We further simulate highly viscous fluids exhibiting the coiling effect using different methods, as shown in Figure 9. Our coupled strategy stably maintains the coiled morphology throughout the simulation. Besides, our method demonstrates more stable coiling behavior compared to the SIMPLE SPH algorithm [Liu et al. 2022].

6.1.3 Comparison of high surface tension fluids. To illustrate the advantage of our strongly coupled approach in simulating fluids with high surface tension, we model fluids with an extremely high surface tension coefficient.

Figure 10 shows the coalescence of two fluid volumes into a single droplet under surface tension. We first implemented the explicit method of [Akinci et al. 2013], which is very unstable under high surface tension. Using the semi-implicit solver based on our method with a decoupled strategy, we achieved stable simulations at high surface tension. However, it still fails when the surface tension is further increased. In contrast, our unified solver, simultaneously coupling incompressibility, viscosity, and surface tension, can stably model the fluid with extremely high surface tension.

Figure 11 presents an extreme simulation scenario involving a highly surface tension dominated fluid. Even when the decoupled semi-implicit surface tension method employs the best solving order validated in Figure 2, it still becomes unstable. In contrast, our unified method, which strongly couples incompressibility, viscosity,

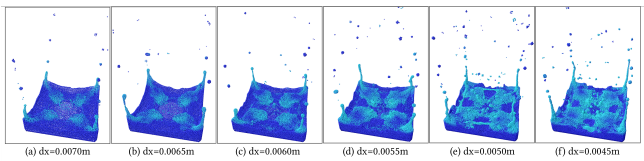

Fig. 13. Dam-break simulation under varying particle spacing (dx). In this scenario, the smoothing lengths are all set to $3dx$, $\kappa = 1.0, \lambda = 0.1, \mu = 0.0, \gamma = 6.0$. The values of dx are labeled under the subfigures, the corresponding particle counts are (a) 24.4k, (b) 29.8k, (c) 35.9k, (d) 50.7k, (e) 68.9k, and (f) 132.7k.

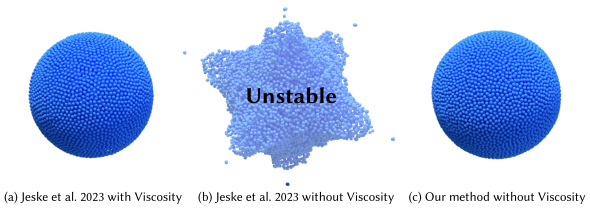

Fig. 14. Comparison with Jeske et al. [2023]. The particle spacings are all $0.01m$, and the smoothing lengths are all $0.04m$. The particle number is 12k. [Jeske et al. 2023] is implemented in SPlisHSPlasH [Bender 2025] and is calculated on the CPU. (a) [Jeske et al. 2023], the viscosity coefficient is 0.15, the surface tension strength is 14000; (b) [Jeske et al. 2023], surface tension strength is 14000, and viscosity coefficient is 0; (c) Our unified method, surface tension strength γ is 1000, viscosity is set to 0, and no additional viscosity is applied.

and surface tension, robustly captures the high-speed collision of high surface tension fluids under large time step size ($1ms$).

6.2 Other comparisons

6.2.1 Different fluids. By assigning different values to key parameters, a variety of fluid types can be simulated by our method, as shown in Figure 5.

6.2.2 Bulk viscosity and shear viscosity. Our method utilizes two independent parameters to control the bulk and shear viscosities, i.e., λ and μ, enabling the simulation of various types of viscous fluids. As shown in Figure 3, increasing shear viscosity weakens the coiling effect of viscous fluids. Figure 12 illustrates simulations of two distinct highly viscous fluids using our approach: melted sugar with obvious buckling and coiling effects, and pitch with a weaker buckling behavior.

6.2.3 Different resolutions. To demonstrate the fluid behaviors under varying particle resolutions, we employ different particle spacings to model the dam break scenario, as shown in Figure 13. While the fluid behaviors under different particle spacings follow similar

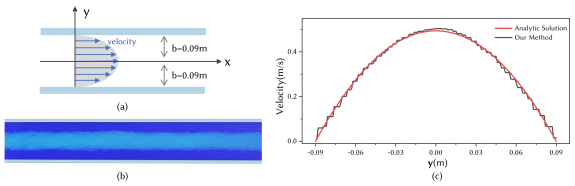

Fig. 15. Poiseuille flow. (a) Schematic of the two-dimensional Poiseuille flow; (b) Steady-state flow (far from the inlet) simulated by our unified method. The particle color is coded by particle velocity. The time step is 0.001s, the particle spacing dx is $0.005m$, $\lambda = 1.0, \mu = 0, \kappa = 1.0, \gamma = 0$; (c) Comparison between our method and the analytical solution. The analytical solution refers to [Takeda et al. 1994], i.e. $\mathbf{v}(y) = \alpha(1 - y^2/b^2)$, where α is the maximum centerline velocity, and b is the channel half-width. The numerical velocity distribution is sampled along the y-axis under steady-state conditions.

Fig. 16. Cream simulations using different strategies (1.7M particles per fluid). (a) Decoupled treatment of viscosity and incompressibility, leads to weak buckling and unstable shape. (b) Our unified method with strong coupling between viscosity and incompressibility, producing rich surface details through robust buckling.

trends, increasing the particle resolution enables the capture of more details of fluid motion.

6.2.4 Comparison with [Jeske et al. 2023]. Figure 14 illustrates the comparison between our method and Jeske et al. [2023]. The method [Jeske et al. 2023] couples the implicit viscosity and surface tension, achieving stable results for high surface tension even with a large time step (Figure 14(a)). However, when the viscosity coefficient of the fluid is set to zero, and XSPH [Monaghan 1989; Schechter and Bridson 2012] is not used, the fluid becomes unstable (Figure 14(b)). This limitation has been discussed in the work of [Jeske et al. 2023]. In contrast, our method can simulate fluids with a similarly high surface tension, even when viscosity is disabled, as shown in Figure 14(c).

6.3 More examples

Figure 15 illustrates the 2D Poiseuille flow simulation conducted using our unified method. In a 2D channel bounded by ghost solid particles, the fluid is driven by a constant inlet velocity. As the flow evolves, the velocity profile along the y-axis gradually stabilizes. We evaluated the transverse velocity distribution (along the y-axis) in the fully developed region and compared it with the analytical solution for steady-state Poiseuille flow [Takeda et al. 1994]. The results demonstrate that our method closely matches the analytical solution.

By varying material parameters, our method can simulate a wide range of fluid behaviors. Figure 1 (left) showcases three representative cases: a low-viscosity fluid, a mud with high viscosity, and a fluid with extremely high surface tension. Figure 16 (b) illustrates highly viscous cream undergoing extrusion, where rich and stable buckling patterns emerge and are stably preserved throughout the simulation; By contrast, the decoupled approach fails to capture fine

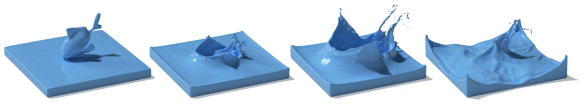

Fig. 17. Water paint (1.1M particles). The low viscous fluid is modeled by our unified method.

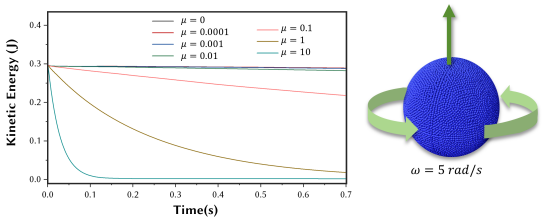

Fig. 18. Kinetic energy curves for the rotating fluid spheres. Fluid spheres with different shear viscosities are given the same initial angular velocity, and the variation curves of particle kinetic energy are obtained under different shear viscosity coefficients μ. In this test, the incompressibility constraint strength is set to $\kappa = 1$, the bulk viscosity strength is set to $\lambda = 20$, and the surface tension strength is set to $\gamma = 200$.

dynamic details of the cream, as shown in Figure 16 (a). Figure 1 (right) illustrates the contrast between high-shear-viscosity mud and low-shear-viscosity cream, demonstrating markedly different behaviors. Figure 17 shows the fine spray of a low-viscosity fluid, simulated using our unified method.

7 Conclusion and Limitations

We introduced a unified variational framework for free-surface flows that incorporates incompressibility, viscosity, and surface tension through nonlocal peridynamics. By consolidating these mechanisms into a single optimization objective, our method eliminates the coupling artifacts and instabilities typical of operator-splitting schemes. Our core contributions include a position-based nonlocal formulation for viscous dissipation that enables consistent nonlinear coupling with density constraints and surface tension, and ensures numerical stability under extreme conditions. Additionally, we derived bulk and shear viscosity models for finer control of different fluids. To solve this variational optimization model of free surface flows stably and efficiently , we utilized the semi-implicit successive substitution method (SISSM). Experimental results demonstrate that our framework achieves superior stability and visual fidelity across a diverse range of scenarios.

Algorithm 1: Nonlocal Unified Solver for Free Surface Flows.

```
while t < t_stop do
    for all particle i do
        x_i ← y_i^n ;
        y_i^* ← x_i + h · (v_i + h · g) ;
        Search neighborhood particles ;
    end
    for k = 0 to N do
        for all particle i do
            Compute y_i^{k+1} (Equation 26) ;
        end
    end
    for all particle i do
        y_i^{n+1} ← y_i^N ;
        v_i^{n+1} ← (y_i^{n+1} − x_i) / h ;
    end
end
```

Table 1. **Statistics.** In these scenarios, the time step size are all 0.001s.

Name	Np[1]	$Iter$[2]	κ[3]	λ[4]	μ[5]	γ[6]	Time[7]
Fig. 1 (Left) Water	661k	5	1	1.5	0	0	43.0ms
Fig. 1 (Left) Mud	153k	40	1	1400	1	600	239ms
Fig. 1 (Left) Mercury	330k	40	1	0.5	0	5000	411ms
Fig. 1 (Right) Mud	1.7M	60	1	700	300	0	2.71s
Fig. 5 (a) Low Viscosity	151k	5	1	0.2	0	0	56.1ms
Fig. 5 (b) High Viscosity	151k	40	1	200	1	0	443ms
Fig. 5 (c) Viscosity Surface Tension	151k	40	1	40	0.1	200	425ms
Fig. 5 (d) High Surface Tension	151k	40	1	0.2	0	1000	417ms
Fig. 8 (a) SIMPLE-1st[7]	10k	89	-	-	-	-	25.2ms
Fig. 8 (b) SIMPLE-20th[8]	10k	1460	-	-	-	-	339ms
Fig. 8 (c) Decoupled	10k	100	10	0	0	0	83.8ms
Fig. 8 (d) Coupled	10k	50	10	0	0	0	56.7ms
Fig. 12 Sugar	50k	60	1	200	0.1	200	203ms
Fig. 12 Pitch	50k	60	1	150	50	0	197ms
Fig. 13 (a) dx = 0.0070	24.4k	20	1	0.1	0	6	35.8ms
Fig. 13 (b) dx = 0.0065	29.8k	20	1	0.1	0	6	44.0ms
Fig. 13 (c) dx = 0.0060	35.9k	20	1	0.1	0	6	52.6ms
Fig. 13 (d) dx = 0.0055	50.7k	20	1	0.1	0	6	69.5ms
Fig. 13 (e) dx = 0.0050	68.9k	20	1	0.1	0	6	96.6ms
Fig. 13 (f) dx = 0.0045	132k	20	1	0.1	0	6	182ms
Fig. 16 (a) Decoupled	1.7M	120	1	2000	0	0	4.12s
Fig. 16 (b) Coupled	1.7M	60	1	2000	0	0	2.87s
Fig. 17 Water paint	1.1M	10	1	0.5	0.0	50	860ms

1. N_p: the number of particles; *2.* $Iter$: iteration counts; *3.* κ: strength of incompressibility constraint; *4.* λ: bulk viscosity coefficient; *5.*μ: the shear viscosity coefficient ; *6.* γ: surface tension coefficient; *7.* "Time": the average computational cost per simulation step for the scenario; *8.* SIMPLE SPH method [Liu et al. 2022] with 1st SIMPLE iteration. The relative error threshold of the viscosity and pressure solvers are both set to 10^{-5}; *9.* SIMPLE SPH method [Liu et al. 2022] with 20 SIMPLE iterations. The relative error threshold of the viscosity and pressure solvers [Liu et al. 2022] are both set to 10^{-5}.

A limitation of our approach is the lack of line search in the semi-implicit solver, which precludes unconditional convergence guarantees. In practice, however, no instability due to this omission was observed, even under extreme conditions. Besides, our shear viscosity, derived from peridynamics, does not decouple the rotational motion from shear deformation, leading to the dissipation of fluid angular momentum. As shown in Figure 18, increased shear viscosity accelerates the dissipation of particle kinetic energy in the rotating fluid.

In future work, we plan to extend the proposed nonlocal variational framework to support additional physical phenomena and models, including viscoelasticity [Li et al. 2025], fluid–solid collision handling [Liu et al. 2026], interfacial forces [Probst and Teschner 2024], and the curvature-derived surface tension model [He et al. 2014], thereby enabling a unified simulation of increasingly complex multiphysics scenarios in a more robust manner. We also aim to generalize the method to a broader class of non-Newtonian fluids, particularly those exhibiting nonlinear viscoelastic behavior [Zhang et al. 2024]. Furthermore, we will investigate an efficient nonlinear optimization solution algorithm or global line-search approach [Lan et al. 2025], to enhance computational efficiency.

Acknowledgments

We would like to thank anonymous reviewers for their valuable advice on improving the paper. This work was supported by the New Generation Artificial Intelligence- National Science and Technology Major Project of China (No. 2025ZD0123902), the National Natural Science Foundation of China (No.92570206, No.62302490), the Key Project of the ISCAS (No. ISCAS-ZD-202401), and the Basic Research Project of ISCAS (No. ISCAS-JCMS-202403).

References

Nadine Abu Rumman, Prapanch Nair, Patric Müller, Loïc Barthe, and David Vanderhaeghe. 2020. ISPH–PBD: coupled simulation of incompressible fluids and deformable bodies. *The Visual Computer* 36, 5 (2020), 893–910.

Stefan Adami, XY Hu, and Nikolaus A Adams. 2010. A new surface-tension formulation for multi-phase SPH using a reproducing divergence approximation. *J. Comput. Phys.* 229, 13 (2010), 5011–5021.

Nadir Akinci, Gizem Akinci, and Matthias Teschner. 2013. Versatile surface tension and adhesion for SPH fluids. *ACM Transactions on Graphics (TOG)* 32, 6 (2013), 1–8.

Nadir Akinci, Markus Ihmsen, Gizem Akinci, Barbara Solenthaler, and Matthias Teschner. 2012. Versatile rigid-fluid coupling for incompressible SPH. *ACM Transactions on Graphics (TOG)* 31, 4 (2012), 1–8.

George Keith Batchelor. 1967. *An introduction to fluid dynamics*. Cambridge university press.

Markus Becker and Matthias Teschner. 2007. Weakly compressible SPH for free surface flows. In *Proceedings of the 2007 ACM SIGGRAPH/Eurographics symposium on Computer animation*. 209–217.

Jan Bender. 2025. SPlisHSPlasH, an open-source library for the physically-based simulation of fluids. https://github.com/InteractiveComputerGraphics/SPlisHSPlasH.

Jan Bender and Dan Koschier. 2016. Divergence-free SPH for incompressible and viscous fluids. *IEEE Transactions on Visualization and Computer Graphics* 23, 3 (2016), 1193–1206.

Michael V Berry. 1971. The molecular mechanism of surface tension. *Physics Education* 6, 2 (1971), 79.

Kenneth Bodin, Claude Lacoursiere, and Martin Servin. 2011. Constraint fluids. *IEEE Transactions on Visualization and Computer Graphics* 18, 3 (2011), 516–526.

Gilles Daviet, Tianchang Shen, Nicholas Sharp, and David IW Levin. 2025. Neurally integrated finite elements for differentiable elasticity on evolving domains. *ACM Transactions on Graphics (TOG)* 44, 2 (2025), 1–17.

Fernando De Goes, Corentin Wallez, Jin Huang, Dmitry Pavlov, and Mathieu Desbrun. 2015. Power particles: an incompressible fluid solver based on power diagrams. *ACM Transactions on Graphics (TOG)* 34, 4 (2015), 50–1.

Luiz Fernando de Souza Andrade, Marcos Sandim, Fabiano Petronetto, Paulo Pagliosa, and Afonso Paiva. 2015. Particle-based fluids for viscous jet buckling. *Computers & Graphics* 52 (2015), 106–115.

Mathieu Desbrun and Marie-Paule Gascuel. 1996. Smoothed particles: A new paradigm for animating highly deformable bodies. In *Computer Animation and Simulation'96: Proceedings of the Eurographics Workshop in Poitiers, France, August 31–September 1, 1996*. Springer, 61–76.

Elie Diaz, Jerry Hsu, Eisen Montalvo-Ruiz, Chris Giles, and Cem Yuksel. 2025. Implicit Position-Based Fluids. In *Proceedings of the SIGGRAPH Asia 2025 Conference Papers*. 1–9.

José Antonio Fernández-Fernández, Fabian Löschner, Lukas Westhofen, Andreas Longva, and Jan Bender. 2025. Symx: Energy-based simulation from symbolic expressions. *ACM Transactions on Graphics (TOG)* 45, 1 (2025), 1–19.

Chris Giles, Elie Diaz, and Cem Yuksel. 2025. Augmented Vertex Block Descent. *ACM Transactions on Graphics (TOG)* 44, 4 (2025), 1–12.

Christoph Gissler, Andreas Peer, Stefan Band, Jan Bender, and Matthias Teschner. 2019. Interlinked SPH pressure solvers for strong fluid-rigid coupling. *ACM Transactions on Graphics (TOG)* 38, 1 (2019), 1–13.

Ryan Goldade, Yipeng Wang, Mridul Aanjaneya, and Christopher Batty. 2019. An adaptive variational finite difference framework for efficient symmetric octree viscosity. *ACM Transactions on Graphics (TOG)* 38, 4 (2019), 1–14.

Xiaowei He, Ning Liu, Sheng Li, Hongan Wang, and Guoping Wang. 2012. Local poisson SPH for viscous incompressible fluids. *Computer Graphics Forum* 31, 6 (2012), 1948–1958.

Xiaowei He, Shusen Liu, Yuzhong Guo, Jian Shi, and Ying Qiao. 2025. A Semi-Implicit SPH Method for Compressible and Incompressible Flows with Improved Convergence. *Computer Graphics Forum* 44, 2 (2025), e70043.

Xiaowei He, Huamin Wang, and Enhua Wu. 2017. Projective peridynamics for modeling versatile elastoplastic materials. *IEEE Transactions on Visualization and Computer Graphics* 24, 9 (2017), 2589–2599.

Xiaowei He, Huamin Wang, Fengjun Zhang, Hongan Wang, Guoping Wang, and Kun Zhou. 2014. Robust simulation of sparsely sampled thin features in SPH-based free surface flows. *ACM Transactions on Graphics (TOG)* 34, 1 (2014), 1–9.

Daniel Holz, Stefan Rhys Jeske, Fabian Löschner, Jan Bender, Yin Yang, and Sheldon Andrews. 2025. Multiphysics simulation methods in computer graphics. *Computer Graphics Forum* (2025), e70082.

Kemeng Huang, Xinyu Lu, Huancheng Lin, Taku Komura, and Minchen Li. 2025. StiffGIPC: Advancing GPU IPC for Stiff Affine-Deformable Simulation. *ACM Transactions on Graphics (TOG)* 44, 3 (2025), 1–20.

Markus Ihmsen, Jens Cornelis, Barbara Solenthaler, Christopher Horvath, and Matthias Teschner. 2013. Implicit incompressible SPH. *IEEE Transactions on Visualization and Computer Graphics* 20, 3 (2013), 426–435.

Stefan Rhys Jeske, Lukas Westhofen, Fabian Löschner, José Antonio Fernández-Fernández, and Jan Bender. 2023. Implicit surface tension for SPH fluid simulation. *ACM Transactions on Graphics (TOG)* 43, 1 (2023), 1–14.

Nahyup Kang and Donghoon Sagong. 2014. Incompressible SPH using the divergence-free condition. *Computer Graphics Forum* 33, 7 (2014), 219–228.

Dan Koschier, Jan Bender, Barbara Solenthaler, and Matthias Teschner. 2020. Smoothed particle hydrodynamics techniques for the physics based simulation of fluids and solids. *arXiv preprint arXiv:2009.06944* (2020).

Dan Koschier, Jan Bender, Barbara Solenthaler, and Matthias Teschner. 2022. A survey on SPH methods in computer graphics. *Computer Graphics Forum* 41, 2 (2022), 737–760.

W Michael Lai, David Rubin, and Erhard Krempl. 2009. *Introduction to continuum mechanics*. Butterworth-Heinemann.

Lei Lan, Zixuan Lu, Chun Yuan, Weiwei Xu, Hao Su, Huamin Wang, Chenfanfu Jiang, and Yin Yang. 2025. JGS2: Near Second-order Converging Jacobi/Gauss-Seidel for GPU Elastodynamics. *ACM Transactions on Graphics (TOG)* 44, 4, Article 44 (July 2025), 15 pages. https://doi.org/10.1145/3731183

Egor Larionov, Christopher Batty, and Robert Bridson. 2017. Variational stokes: A unified pressure-viscosity solver for accurate viscous liquids. *ACM Transactions on Graphics (TOG)* 36, 4 (2017), 1–11.

Ruolan Li, Yanrui Xu, Yalan Zhang, Jiri Kosinka, Alexandru C Telea, Jian Chang, Jian Jun Zhang, Xiaojuan Ban, and Xiaokun Wang. 2025. Multiphase Particle-Based Simulation of Poro-Elasto-Capillary Effects. In *Proceedings of the SIGGRAPH Asia 2025 Conference Papers*. 1–11.

Junyuan Liu, Shusen Liu, Yuzhong Guo, Ruikai Liang, Yin Li, and Xiaowei He. 2026. A Semi-Analytical Energy Model for Particle-Based Fluid Simulation Involving Complex Moving Boundaries. *Computer Graphics Forum* (2026), e70333.

Shusen Liu, Yuzhong Guo, Ying Qiao, and Xiaowei He. 2025. An Adaptive Particle Fission-Fusion Approach for Dual-Particle SPH Fluid. In *Pacific Graphics Conference Papers*. The Eurographics Association. https://doi.org/10.2312/pg.20251269

Shusen Liu, Xiaowei He, Yuzhong Guo, Yue Chang, and Wencheng Wang. 2024. A dual-particle approach for incompressible SPH fluids. *ACM Transactions on Graphics (TOG)* 43, 3 (2024), 1–18.

Shusen Liu, Xiaowei He, Wencheng Wang, and Enhua Wu. 2022. Adapted SIMPLE algorithm for incompressible SPH fluids with a broad range viscosity. *IEEE Transactions on Visualization and Computer Graphics* 28, 9 (2022), 3168–3179.

Jia-Ming Lu and Shi-Min Hu. 2025. Reliable Iterative Dynamics: A Versatile Method for Fast and Robust Simulation. *ACM Transactions on Graphics (TOG)* 44, 3 (2025), 1–18.

Zixuan Lu, Xiaowei He, Yuzhong Guo, Xuehui Liu, and Huamin Wang. 2023. Projective peridynamic modeling of hyperelastic membranes with contact. *IEEE Transactions on Visualization and Computer Graphics* 30, 8 (2023), 4601–4614.

Miles Macklin and Matthias Müller. 2013. Position based fluids. *ACM Transactions on Graphics (TOG)* 32, 4 (2013), 1–12.

Miles Macklin, Matthias Müller, and Nuttapong Chentanez. 2016. XPBD: position-based simulation of compliant constrained dynamics. In *Proceedings of the 9th International Conference on Motion in Games*. 49–54.

JJ Monaghan. 1989. On the problem of penetration in particle methods. *J. Comput. Phys.* 82, 1 (1989), 1–15.

Matthias Müller, David Charypar, and Markus Gross. 2003. Particle-based fluid simulation for interactive applications. In *Proceedings of the 2003 ACM SIGGRAPH/Eurographics symposium on Computer animation*. 154–159.

Prapanch Nair and Gaurav Tomar. 2014. An improved free surface modeling for incompressible SPH. *Computers & Fluids* 102 (2014), 304–314.

Suhas Patankar. 2018. *Numerical heat transfer and fluid flow*. CRC press.

Andreas Peer, Markus Ihmsen, Jens Cornelis, and Matthias Teschner. 2015. An implicit viscosity formulation for SPH fluids. *ACM Transactions on Graphics (TOG)* 34, 4 (2015), 1–10.

Andreas Peer and Matthias Teschner. 2016. Prescribed velocity gradients for highly viscous SPH fluids with vorticity diffusion. *IEEE Transactions on Visualization and Computer Graphics* 23, 12 (2016), 2656–2662.

Timo Probst and Matthias Teschner. 2023. Monolithic friction and contact handling for rigid bodies and fluids using SPH. *Computer Graphics Forum* 42, 1 (2023), 155–179.

Timo Probst and Matthias Teschner. 2024. Unified Pressure, Surface Tension and Friction for SPH Fluids. *ACM Transactions on Graphics (TOG)* 44, 1 (2024), 1–28.

Ziyin Qu, Minchen Li, Fernando De Goes, and Chenfanfu Jiang. 2022. The power particle-in-cell method. *ACM Transactions on Graphics (TOG)* 41, 4 (2022).

Lixin Ren, Shusen Liu, Yuzhong Guo, and Enhua Wu. 2023. Algebraic Adaptive Signed Distance Field on GPU. In *The 11th international conference on Computational Visual Media (CVM 2023)*. https://api.semanticscholar.org/CorpusID:260141046

Hagit Schechter and Robert Bridson. 2012. Ghost SPH for animating water. *ACM Transactions on Graphics (TOG)* 31, 4 (2012), 1–8.

Stewart A Silling. 2000. Reformulation of elasticity theory for discontinuities and long-range forces. *Journal of the Mechanics and Physics of Solids* 48, 1 (2000), 175–209.

Stewart A Silling, Michael Epton, Olaf Weckner, Jifeng Xu, and E23481501120 Askari. 2007. Peridynamic states and constitutive modeling. *Journal of elasticity* 88, 2 (2007), 151–184.

Breannan Smith, Fernando De Goes, and Theodore Kim. 2018. Stable neo-hookean flesh simulation. *ACM Transactions on Graphics (TOG)* 37, 2 (2018), 1–15.

B. Solenthaler and R. Pajarola. 2009. Predictive-corrective incompressible SPH. *ACM Transactions on Graphics (TOG)* 28, 3, Article 40 (July 2009), 6 pages. https://doi.org/10.1145/1531326.1531346

Tetsuya Takahashi, Yoshinori Dobashi, Issei Fujishiro, Tomoyuki Nishita, and Ming C Lin. 2015. Implicit formulation for SPH-based viscous fluids. *Computer Graphics Forum* 34, 2 (2015), 493–502.

Tetsuya Takahashi, Yoshinori Dobashi, Tomoyuki Nishita, and Ming C Lin. 2018. An efficient hybrid incompressible SPH solver with interface handling for boundary conditions. *Computer Graphics Forum* 37, 1 (2018), 313–324.

Hidenori Takeda, Shoken M Miyama, and Minoru Sekiya. 1994. Numerical simulation of viscous flow by smoothed particle hydrodynamics. *Progress of theoretical physics* 92, 5 (1994), 939–960.

Alexandre Tartakovsky and Paul Meakin. 2005. Modeling of surface tension and contact angles with smoothed particle hydrodynamics. *Physical Review E—Statistical, Nonlinear, and Soft Matter Physics* 72, 2 (2005), 026301.

Jiamin Wang, Haoping Wang, Xiaokun Wang, Yalan Zhang, Jiří Kosinka, Steffen Frey, Alexandru Telea, and Xiaojuan Ban. 2025. Peridynamics-based simulation of viscoelastic solids and granular materials. *Computers & Graphics* (2025), 104463.

Marcel Weiler, Dan Koschier, Magnus Brand, and Jan Bender. 2018. A physically consistent implicit viscosity solver for SPH fluids. *Computer Graphics Forum* 37, 2 (2018), 145–155.

Frank M White and Joseph Majdalani. 2006. *Viscous fluid flow*. Vol. 3. McGraw-Hill New York.

Han Yan and Bo Ren. 2023. High Density Ratio Multi-Fluid Simulation with Peridynamics. *ACM Transactions on Graphics (TOG)* 42, 6 (2023), 1–14.

Tao Yang, Ralph R Martin, Ming C Lin, Jian Chang, and Shi-Min Hu. 2017. Pairwise force SPH model for real-time multi-interaction applications. *IEEE Transactions on Visualization and Computer Graphics* 23, 10 (2017), 2235–2247.

Jingqi Zhang, Zihao Zhou, Lixin Ren, Junyuan Liu, Ying Li, and Xiaowei He. 2025. A Parallel Multiscale FIM Approach in Solving the Eikonal Equation on GPU. *Computer-Aided Design* (2025), 103949.

Yalan Zhang, Shen Long, Yanrui Xu, Xiaokun Wang, Chao Yao, Jiri Kosinka, Steffen Frey, Alexandru Telea, and Xiaojuan Ban. 2024. Multiphase Viscoelastic Non-Newtonian Fluid Simulation. *Computer Graphics Forum* 43, 8 (2024), e15180.

Jiangming Zhao, Adam Larios, and Florin Bobaru. 2022. Construction of a peridynamic model for viscous flow. *J. Comput. Phys.* 468 (2022), 111509. https://doi.org/10.1016/j.jcp.2022.111509

Qizhi Zhu and Tao Ni. 2017. Peridynamic formulations enriched with bond rotation effects. *International Journal of Engineering Science* 121 (2017), 118–129. https://doi.org/10.1016/j.ijengsci.2017.09.004